Physica B 427 (2013) 76–84

Contents lists available at SciVerse ScienceDirect

Physica B

journal homepage: www.elsevier.com/locate/physb

Binary cluster collision dynamics and minimum energy conformations

Francisco Muñoz [a,b,c], José Rogan [b,c], J.A. Valdivia [b,c], A. Varas [b,d], Miguel Kiwi [b,c,*]

[a] Max Planck Institute of Microstructure Physics, Weinberg 2, 06120 Halle, Germany
[b] Departamento de Física, Facultad de Ciencias, Universidad de Chile, Santiago, Chile
[c] Centro para el Desarrollo de la Nanociencia y Nanotecnología, CEDENNA, Avenida Ecuador 3493, Santiago, Chile
[d] Nano-Bio Spectroscopy Group, ETSF Scientific Development Centre, Departamento de Física de Materiales, Universidad del País Vasco UPV/EHU, Av. Tolosa 72, E-20018 San Sebastián, Spain

ARTICLE INFO

Article history:
Received 3 April 2013
Received in revised form
26 June 2013
Accepted 27 June 2013
Available online 4 July 2013

Keywords:
Coinage metal clusters
Cluster collisions
Electronic structure of nanoscale materials
DFT molecular dynamics

ABSTRACT

The collision dynamics of one Ag or Cu atom impinging on a Au_{12} cluster is investigated by means of DFT molecular dynamics. Our results show that the experimentally confirmed 2D to 3D transition of $Au_{12} \rightarrow Au_{13}$ is mostly preserved by the resulting planar $Au_{12}Ag$ and $Au_{12}Cu$ minimum energy clusters, which is quite remarkable in view of the excess energy, well larger than the 2D–3D potential barrier height. The process is accompanied by a large $s-d$ hybridization and charge transfer from Au to Ag or Cu. The dynamics of the collision process mainly yields fusion of projectile and target, however scattering and cluster fragmentation also occur for large energies and large impact parameters. While Ag projectiles favor fragmentation, Cu favors scattering due to its smaller mass. The projectile size does not play a major role in favoring the fragmentation or scattering channels. By comparing our collision results with those obtained by an unbiased minimum energy search of 4483 $Au_{12}Ag$ and 4483 $Au_{12}Cu$ configurations obtained phenomenologically, we find that there is an extra bonus: without increase of computer time collisions yield the planar lower energy structures that are not feasible to obtain using semi-classical potentials. In fact, we conclude that phenomenological potentials do not even provide adequate seeds for the search of global energy minima for planar structures. Since the fabrication of nanoclusters is mainly achieved by synthesis or laser ablation, the set of local minima configurations we provide here, and their distribution as a function of energy, are more relevant than the global minimum to analyze experimental results obtained at finite temperatures, and is consistent with the dynamical coexistence of 2D and 3D liquid Au clusters conformations obtained previously.

1. Introduction

The study of nanosized alloys has become an active area of science and technology. Actually, nanoalloys pose a challenge to a wide range of specialists, ranging from chemists and physicists to engineers, since the mechanical and electrical properties of nanoalloys strongly depend on the spatial arrangement the atoms adopt when forming the cluster. Also the catalytic activity, which is important in many industrial processes, is largely determined by the cluster structure [1–5]. Of particular interest in this context are the coinage metals in general and gold in particular, which up to 13 atoms tend to form planar clusters. Even the substitution of a single gold atom, by another noble metal, opens the possibility to tailor the 0.8 eV energy barrier of the 2D to 3D transition [6]. Still another possibility to control this transition is to match or mismatch the atomic size, for example, by substitution of Au with either Ag or Cu.

Consequently, sorting out the most significant ingredients that decide the conformation that a cluster does adopt constitutes a pertinent objective. However, the task is quite formidable since the number of different configurations grows exponentially with the number of atoms. When dealing with alloys, even just binary ones, the challenge becomes significantly more arduous, due to the fact that the many ways the different species can be distributed in the cluster increases enormously the already large number of possible conformations that a pristine sample can adopt.

On the other hand, some time ago Mariscal et al. [7] found that the simulation of collision processes, by means of classical molecular dynamics, constitutes an efficient method to generate a diverse set of bimetallic nanocluster structures with different chemical compositions. Originally, the collision of gold clusters by classical molecular dynamics techniques was carried out by Rogan et al. [8]. More recently the same problem, for pristine gold and rhodium cluster collisions, was re-examined by means of density functional theory molecular dynamics (DFT-MD) [9,10], and it was established that the

* Corresponding author at: Departamento de Física, Facultad de Ciencias, Universidad de Chile, Santiago, Chile. Tel.: +56 2 2978 7290; fax: +56 2 2271 2973.
E-mail address: m.kiwi.t@gmail.com (M. Kiwi).

0921-4526/$ - see front matter © 2013 Elsevier B.V. All rights reserved.
http://dx.doi.org/10.1016/j.physb.2013.06.036

minimum energy configurations that are obtained using classical and DFT-MD often are very significantly different. This is mainly due to the polarization caused by the charge rearrangement of the electronic cloud during the collision process.

In these previous studies [9,10], it was found that the target fragmentation and projectile scattering can be classified in two broad groups: an almost instantaneous fragmentation, and a process mediated by successive atomic rearrangements. The first group is more likely for large impact parameter collisions or when the projectile impacts head-on one of the target atoms, which then detaches from the cluster with a minimal atomic rearrangement. The other possible outcome occurs when the projectile energy is spread out over the whole cluster, setting it into oscillation. Remarkably, when a gold atom is on its way to ejection from this excited state configuration, the cluster adapts its shape and pulls this escaping atom back in. This behavior gives rise to a notorious expansion of the cluster, which often adopts a flake-like shape (even for energies more than one order of magnitude larger than the 2D to 3D barrier [6]), or even a linear-like shape. Moreover, when studying the collision processes of Rh clusters [10], effects due to the cluster dynamics on the collision outcome are quite important. In this case, allowing or neglecting for spin-polarization yields a slower or faster cluster dynamics, respectively. This difference in the system dynamics translates into the absence of scattering for the unpolarized spin case. Summarizing, the characteristics of the dynamics are quite relevant to the collision outcome, especially for gold on gold where the motion of the cluster atoms seems to be collectively coordinated to retain their constituent atoms. The physics behind this phenomenon is related to the rather weak metallic *s*-bonding, as compared with *d*-bonded Rh clusters, and the slow motion of the massive Au fragments, which allows sufficient time for the main cluster to recapture them.

In this paper we focus on the dynamics of the collision process and compare the binary configurations thus obtained, after a DFT relaxation, with the results that were calculated by refining, also by means of DFT methods, the minimum energy structures generated by the Fast Inertial Relaxation Algorithm (FIRE) based procedure using phenomenological potentials. The FIRE algorithm is a novel and efficient algorithm to determine a potential minimum, put forward by Bitzek et al. [11] who describe it as a method based on conventional molecular dynamics, with additional velocity modifications and adaptive time steps.

Thus, the main objectives of the collision study are: (i) to obtain a deeper insight into the dynamics of the collision process, and the stability and energy distribution of the resulting fragments, and (ii) to generate minimum energy conformations of binary nanoclusters. For the latter we bombard gold clusters with isoelectronic noble metal projectile atoms, namely silver and copper, which have a $d^{10}s^1$ outer shell. Both elements are in the same column of the periodic table and are lighter than Au. Therefore, the dynamics decouples into two time scales, the Ag or Cu time scale, and the Au one. Apart from the atomic mass, there is another important difference between Ag and Cu: their size. This allows us to study the evolution of size matched (Au–Ag) and mismatched (Au–Cu) clusters. In spite of the fact that the Ag and Cu have an iso-electronic $d^{10}s^1$ outermost shell, they behave quite differently from Au. For example, due to the strong Au $s-d$ hybridization the minimal energy Au_{12} cluster is planar (the possible planar ground-state of Au_{13} and Au_{14} is still the subject of controversy [12–15]) while for Ag and Cu the 2D to 3D transition occurs at a size of just 8 atoms. Moreover, pristine Ag and Cu small clusters have the same ground-state motifs [16].

This paper is organized as follows: after this introduction we present the method and the details of the DFT calculations in Section 2. In Section 3 we describe the collision setup and the dynamics proper. In Section 4 we focus on the results for the bimetallic clusters, providing a detailed analysis of the lowest energy binary conformations we obtain. In Section 5 we compare the configurations obtained through the cluster collision processes with those attained by means of the DFT refinement of the massive FIRE results. Section 6 closes the paper with a summary of our results and the implications they have for the description and interpretation of experiments.

2. Method and computational details

Cluster collisions are simulated using the DFT formalism [17,18] as implemented in the VASP code [19–21]. In order to avoid self-interactions, or even worse, spurious interactions between fragments scattered after the collision, we use the largest possible simulation cell compatible with our computational resources (*i.e.* a cube with 18 Å edges). In addition, we treat the fragments separately when they are sufficiently apart for their interaction to become negligible. The simulation box size was monitored to insure that the images are more than 7.5 Å apart, a criterion that insures that the forces between images are small. Actually, we checked that already for a separation of 6.5 Å the forces are ~0.01 eV which is within the error of our calculations. In some rare instances, when fragmentation occurred, the images became too close and the simulation box was resized to satisfy the 7.5 Å minimum separation. PAW pseudo-potentials [22] and PBE [23] for the exchange-correlation are used. The energy cutoff was set to 270 eV. The target we choose is the putative minimum energy configuration of the Au_{12} cluster. Fortunately, these gold clusters, as well as others of different sizes, have been widely studied at the DFT level and reported in the literature [14,16,24–30], and we made sure that our initial set of parameters yields an adequate description of them. However, preliminary calculations hint that the results of the collision process are not very sensitive on the adoption of a minimal energy target.

Although our targets are nonmagnetic, the atomic rearrangement during the collision process could give rise to *s*-like ferromagnetism of noble metal clusters with icosahedral symmetry, as pointed out by Luo et al. [31]. However, in a previous study it was found that for gold clusters [9] the spin-polarization does not play a major role in the collision dynamics. It is well known that for Au the spin–orbit coupling plays an important role [32], since the inclusion of the spin–orbit coupling in the calculations does shift the binding energies. However, the changes it induces, both in the structure and the relative energies, are negligible [13]. Thus for our purposes, as long as we limit our attention to projectile energies $E_K \geq 1$ eV, we can safely ignore spin–orbit coupling in our calculations.

The collisions are setup as follows: first we choose a proper collision target (*i.e.* a cluster in the minimum energy configuration) which is positioned at the origin of the simulation box (see Fig. 1). The projectile is located a safe distance away from the cluster and impinges normally to the target plane. We limit our attention to a Au_{12} cluster aligned in such a way as to maximize its cross section. The impact parameter b is measured in Å relative to the cluster center of mass (as illustrated by the bar in Fig. 1). The target has no initial center of mass velocity and no vibrational energy (*i.e.* $T=0$ K). Next, the projectile -a Ag or Cu atom- is placed at $\approx 7.0\,\text{Å}$ from the nearest target atom. The projectile carries a kinetic energy E_K and flies toward the target with an impact parameter b. The dynamics are followed during a time of 2 ps, conserving the total energy (*i.e.* the simulation is carried out in the micro-canonical ensemble). This way the system initially evolves freely during 2 ps, just constrained by energy conservation.

After the collision takes place, and depending on the values of both E_K and b, we contemplate one of the following three scenarios:

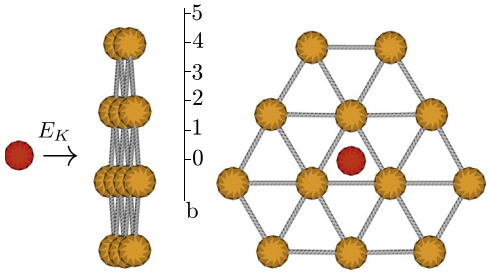

Fig. 1. Lateral and frontal views of the Au_{12} target and the projectile. The target atoms are colored yellow and the projectile red. The various impact parameters (b values), measured in Å relative to the center of mass, are given on the right. The projectile is an iso-electronic Ag or Cu atom. (For interpretation of the references to color in this figure caption, the reader is referred to the web version of this article.)

fusion of target and projectile, target fragmentation, or projectile scattering. It may be worth mentioning that at least another possibility does exist: evaporation. If we estimate a cluster temperature value on the basis of the vibration kinetic energy of the atoms, a concept which certainly is far from rigorous for our small clusters, we can establish an energy scale that is helpful in order to develop a qualitative understanding of the processes. The temperature defined in this way, which the cluster gains after impact, in several cases surpasses the bulk boiling temperature. In some of these events we obtain that a few atoms are expelled during the late stages of the dynamics (*i.e.* after 2 ps). These events are difficult to label as fragmentation or evaporation, and in the next section we will elaborate on this matter, when we discuss the collision dynamics. Certainly, after the collision takes place the target is left in an excited (high temperature) state and to systematize our analysis of the data, and to be able to find candidates for minimum energy configurations, it is necessary to get rid of this excess excitation energy. Thus, we simulate a radiation process, or cooling down of the system after collision, by linearly rescaling the atomic velocities until they reach room temperature, which takes an additional time of around 3 ps. Finally a direct optimization of the final structures is carried out, until all the inter-atomic forces are less than 0.01 eV/Å.

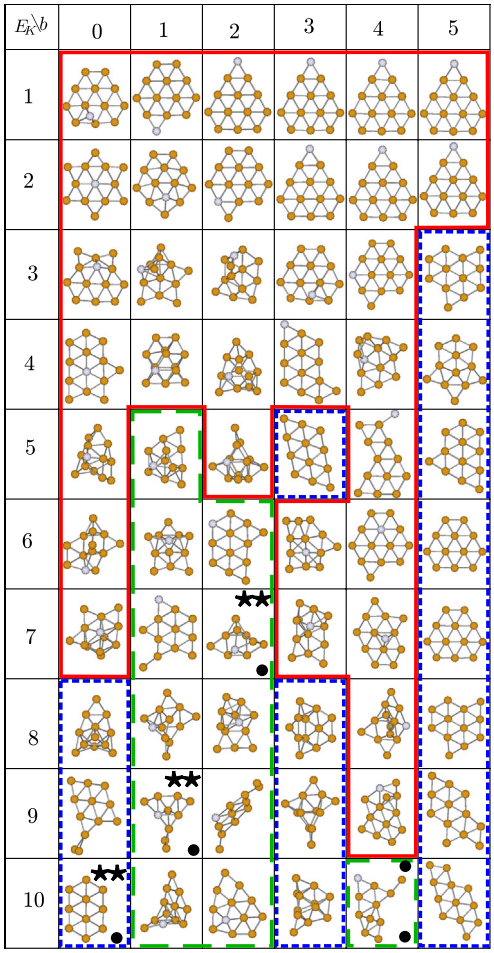

Fig. 2. Conformations resulting from the collision of a Ag atom projectile on a Au_{12} target. The configurations correspond to structures cooled down to 300 K. The impact parameter b, indicated at the top in Å, is measured relative to the center of mass of the target. The kinetic energy of the projectile E_K is given on the left in eV. The red (continuous), green (long dash) and blue (short dash) frames denote fusion, fragmentation and scattering, respectively. In the fragmentation region when a single atom is expelled, either a cluster atom or the projectile, no symbol is drawn, while a full black circle • indicates that a Ag and a Au atom have broken away from the cluster. The ⋆⋆ symbol denotes a dimer. The Au (Ag) atoms are yellow (light-gray).

3. Collision results

The cluster conformations that are obtained, after the collision and cooling processes take place, are displayed in Figs. 2 and 3. They correspond to a Ag or a Cu atom projectile, respectively, impinging on the 12 atom gold cluster illustrated in Fig. 1. As mentioned before we limit our interest to three scenarios: (i) fusion, defined as the binding of projectile and target, to form $Au_{12}Ag$ or $Au_{12}Cu$; (ii) scattering, when the projectile does not bind to the target, and the target after collision remains as a Au_{12} cluster but in an excited state; and, (iii) fragmentation, which occurs when one or more of the target atoms breaks away from the cluster. In both figures these three regimes (fusion, scattering, and fragmentation) are enclosed by red (continuous), blue (short dash), and green (long dash) frames, respectively.

Inspection of Figs. 2 and 3 shows that fusion is dominant, especially for low energy E_K and small impact parameter. Compared with the Au on Au collision [9] -where scattering events are scarce- we conclude that the less massive the projectile the more frequently scattering occurs. This statement can be intuitively understood on the basis of momentum conservation

$$v_p^r = v_p - \frac{M_T}{m_p} V_T, \tag{1}$$

where v_p (v_p^r) is the projectile initial (recoil) velocity, V_T is the target (initially at rest) recoil velocity, M_T and m_p are the target and projectile masses. The recoil velocity depends on the mass ratio and is inversely proportional to the projectile mass. However, this simple argument has limited validity, since V_T depends on the specific way the energy is delivered to the target (*i.e.* how much energy is transferred to internal excitations). Moreover, the projectile escape velocity depends on both impact parameter and the species of the projectile.

An interesting feature of the scattering and/or fragmentation outcome is its b dependence. When the projectile impacts a target atom quasi-head-on its detachment is almost instantaneous for $b=1$ and 2 Å. However, the projectile does not "just take the place of the missing atom", but it wanders around the target. On the other hand, if the impact takes place at the center of a "hole", *i.e.* the projectile impacts on a three-fold coordinated site ($b=0$ or 3 Å) the projectile energy not only spreads over three atoms, but also the momentum transfer to them is oblique, hindering their rearrangement. This way, the projectile comes to a full stop -since it is not capable of breaking the target- and recoils with only a fraction of its initial energy. This kinetic energy implies a slow Ag, and a faster Cu recoil, due to their different masses, and brings

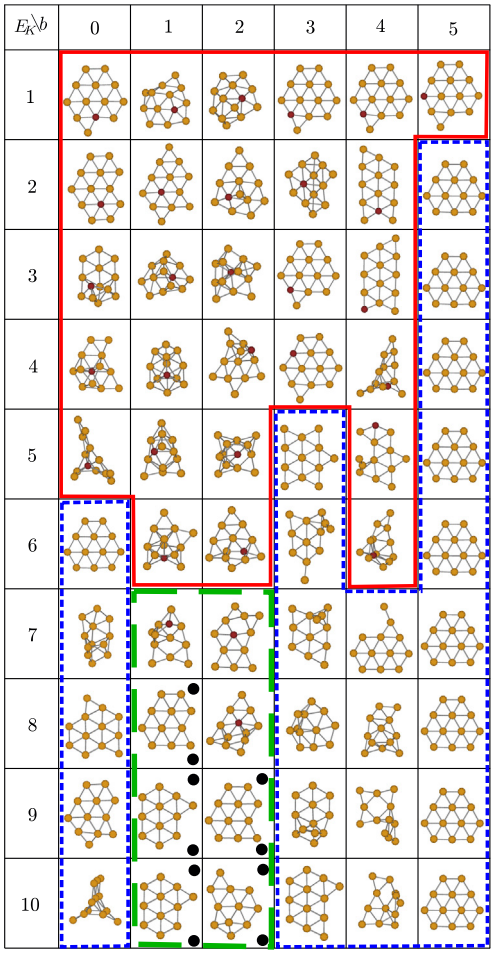

Fig. 3. Cu projectile on a Au target. The configurations that are drawn correspond structures cooled down to 300 K. The impact parameter b, indicated at the top in Å, is measured relative to the center of mass of the target. The kinetic energy of the projectile E_K is given at the left in eV. The red (continuous), green (long dash) and blue (short dash) frames denote fusion, fragmentation and scattering, respectively. In the fragmentation region two separate full black circles • indicate that one Cu and one Au atom have broken away from the cluster, otherwise only one atom is expelled. If a single atom is expelled, either a cluster atom or the projectile, no symbol is drawn. The Au (Cu) atoms are yellow (brown).

about a reduction of the E_K value to obtain scattering. Also, this explains the absence of scattering when the projectile is a Au atom [9], which is too slow to avoid recapture by the excited target. For $b=4$ Å the situation is different, since there are just two less coordinated (easy to rearrange) gold atoms and no single atom to detach.

It is worth pointing out that there are two time scales: a fast one, related to the magnitude of the momentum transfer, and a slower time scale governed by the magnitude of the cluster rearrangement velocities. The former is relevant to the collision outcome (fragmentation or scattering). The latter determines the dynamics of the atomic rearrangement process, and thus the final configuration that is attained, as the dopant finds its optimum position in the cluster. The difference between momentum and projectile velocity magnitudes is due to the different Ag and Cu masses.

However, some mixed scenarios also emerge, as is the case for ($b=1$ Å, $E_K\geq 8$ eV), ($b=2$ Å, $E_K\geq 9$ eV), where scattering and fragmentation occur simultaneously (*i.e.* Au_{11}+Cu+Au). In order to keep Figs. 2 and 3 as simple as feasible we have assigned these cases to fragmentation. In addition, in Fig. 2 we notice that a silver atom projectile can eject a Au dimer, after significant cluster rearrangement. It is not clear if this happens because of impact driven cluster fragmentation or evaporation, due to a large temperature increase.

When a Ag or a Cu atom impinges on the Au_{12} configuration it is apparent that, within the parameter space that we investigated, fusion (red continuous frame) is the dominant collision outcome up to $E_K\sim 5$ eV, except for large impact parameters. For larger E_K values the tendency is toward target fragmentation and scattering. With the Ag projectile the rate for both processes is similar, but for the Cu projectile scattering is widely favored over fragmentation events, since the E_K needed by a Cu atom to break the target is larger. Even for $b=1$ Å and $E_K\geq 8$ eV the fragmentation is accompanied by the scattering of the projectile, since the recoil is too fast to allow for capture by the target, after detaching a Au atom. Compared with the Au on Au collision [9] -where the scattering events are scarce-, we conclude that the less massive the projectile the more frequent is the scattering. This increase in the scattering rate is balanced by a reduction of fusion and fragmentation events.

The appearance in Fig. 2 of an isolated scattering event for a Ag projectile with $b=3$ Å and $E_K=5$ eV deserves a closer look, since it is caused by a different mechanism than the scattering events at higher energies. In Fig. 4 some selected frames, for four relevant energies $E_K=4$, 5, 6 and 8 eV, denoted as (A, first frame upper row), (B, three frames upper row), (C, three frames lower row) and (D, last frame lower row), respectively, are given. The black long headed arrows denote the forces on the projectile, and the empty triangular headed arrows, on the right hand side frames, illustrate its velocity. In all of them the first frame corresponds to an instant after the impact (first impact) takes place, showing how the projectile bounces, leading in some instances to a second impact. The simplest case to study is (D): the projectile recoils after the impact with enough velocity to escape, and at $t_0=500$ fs the projectile has a finite velocity but it is too far away to be attracted back to the target. The opposite behavior is observed in (A), where the projectile gains some recoil velocity and soon ($t_0=400$ fs thereafter) it has exhausted its kinetic energy and is recaptured by the main cluster in a second weak collision. A similar scenario develops for cases (B) and (C), with the difference that the projectile flies for a longer time as its kinetic energy tends to zero. Actually, in case (C) the restoring pulling force it experiences is minimal, such that at time $t_1=948$ fs the projectile comes to a full-stop. But, there exists still another difference which turns out to be more important than the magnitude of the force. In (B) the projectile hits a single target atom head on, but the impact is not strong enough to fragment the target, just sending the impacted atom backward while the cluster moves away from the projectile. Instead, in (C) the second impact is over a three-fold coordinated site, with a stronger attraction between target and projectile, so that a large fraction of the energy spreads over the whole cluster, hindering the target recoil velocity. In the end the differences of the atomic scale dynamics of this second collision yield a radically different outcome: in (B) the projectile escapes; while in (C), at $t_2=1616$ fs, we observe that it is pulled-back into the cluster.

A novel feature found for the collision outcome, only present when a Ag atom is the projectile, is the late detachment of a Au dimer from the excited cluster (events marked with stars in Figs. 2 and 3). In these cases the dimer is expelled at the beginning of the cooling process (*i.e.* after the 2 ps assigned to the collision stage). The classification of these events as either a fragmentation or as an early evaporation is not clear-cut. It is worth stressing that in the remaining cases (and for the collisions of Au on Au, and of Rh on Rh clusters) the classification of an event as fragmentation and/or scattering instead of evaporation is completely unambiguous [9,10]. To complicate things even further in all these late detachment events another atom was expelled (*i.e.* prior to the dimer detachment and shortly after impact), during a regular fragmentation event. The relevance of this scenario is that the

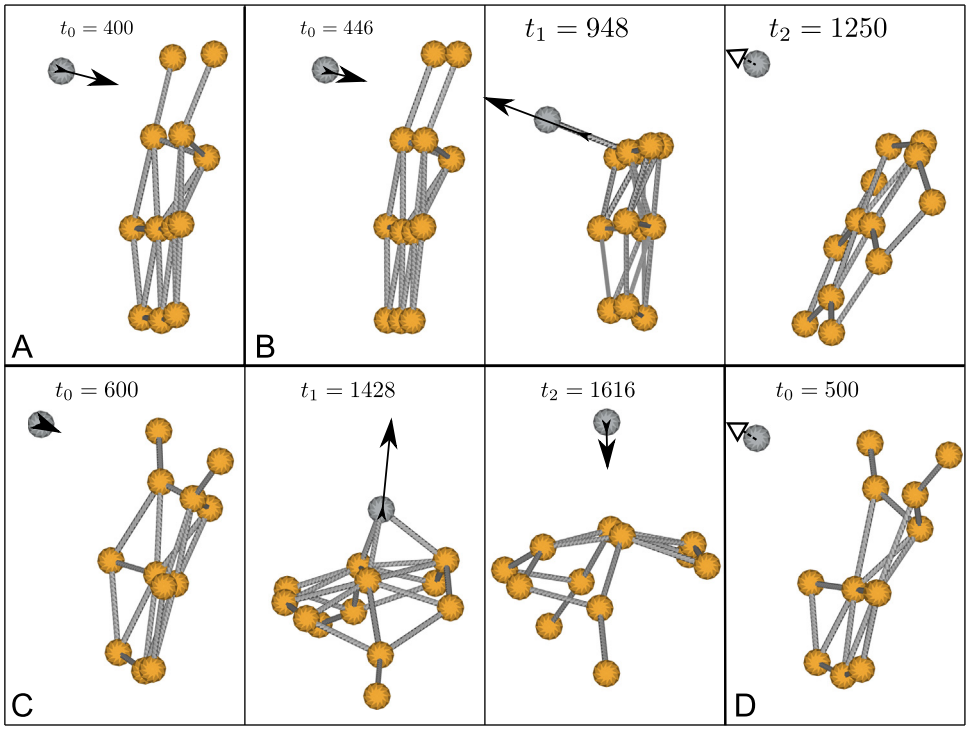

Fig. 4. Selected frames of the collision of Ag on the Au_{12} target. The impact parameter is always $b=3$ Å. The energy $E_K = 4$, 5, 6 and 8 eV for A (one frame), B (three frames), C (three frames) and D (one frame), respectively. At the top of each frame the elapsed simulation time is given in femtoseconds. The long black headed arrows denote the total force over the projectile atom. The empty smaller triangular headed arrows on the right hand side denote the velocity. The scale of the vectors is arbitrary, but representative of the physics. Absence of force or velocity vector means a null vector.

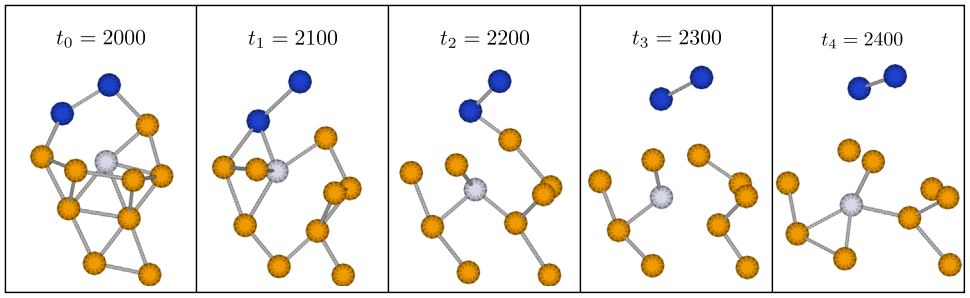

Fig. 5. Dynamics of the expulsion of a Au dimer by a Ag projectile ($b=1$ Å, $E_K=9$ eV). The outgoing dimer is colored blue (dark). It can be seen that the Au atoms surrounding the Ag are 'slow' and fail to recapture the fleeing dimer. The time unit is femtoseconds. (For interpretation of the references to color in this figure caption, the reader is referred to the web version of this article.)

expelled atom carries away 10% of the incoming kinetic energy E_K for ($b=0$, $E_K=10$ eV); 61% for ($b=1$ Å, $E_K=9$ eV), and 27% for ($b=1$ Å, $E_K=7$ eV). Although we do not have a complete explanation for this behavior, it suggests that a small Ag concentration can lower the boiling temperature of a AuAg cluster. A closer inspection of the frames (see Fig. 5) shows that the dynamics of the gold atoms near the Ag one are largely influenced by it, and that they are also faster, leaving them "misplaced" and slow to interact and recapture the remaining gold atoms. This behavior also is observed for ($b=0$, $E_K=10$ eV), since despite the prior scattering of the Ag atom the remaining gold atoms are left "misplaced" and unable to recapture the departing dimer.

The projectile species, either Ag or Cu, play a key role in the dynamics that develops after impact. The smaller masses yield several features that are unique for the bimetallic case. While during the dynamics the Au atoms have a small net displacement, except for the atomic rearrangement immediately after impact, the Ag or Cu atoms wander around the gold cluster *i.e.*: often changing neighborhood, often wandering to the cluster borders. This behavior appears to be due to their lower mass which allows for a faster dynamics, and therefore the Ag or Cu atoms are capable of interacting with the Au atoms in their neighborhood that are prone to escape. However, Ag and Cu have an important difference: their size. Since the Cu atoms are smaller (and faster) than Au, they can penetrate into the gold cluster by easily breaking Au–Au bonds. The mechanism is simple: the Cu atom approaches a Au atom and pushes apart some of the Au neighbors. Since the Cu atom carries some excess kinetic energy it keeps moving, breaking a Au–Au bond. The tendency to wander around the cluster gives the Ag atom a lower average coordination than the Au atoms (2.7 versus 3.5, when averaging over the first 2 ps for events with fusion outcome). The additional effectiveness of Cu to break the Au bonds allows for a higher coordination than that of Au (3.9 versus 3.5, when averaging over the first 2 ps of events leading to fusion). The coordination is computed as the number of atoms within $1.1 \times d_{NN}$, where d_{NN} is the bulk nearest neighbor distance. This coordination tendency is reflected in Figs. 2 and 3, and is preserved even after cooling. While Ag prefers to have less neighbors, Cu prefers a more central location, which is in agreement with the results reported by Rapallo et al. [33] and by Rossi et al. [34].

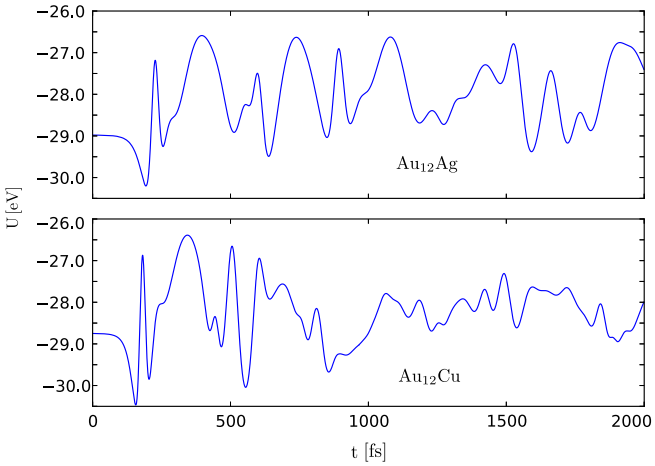

Fig. 6. Time evolution of the potential energy U as a function of time t for single Ag (upper panel) and Cu atoms (lower panel) colliding with a Au_{12} cluster. The atom impacts the cluster center of mass ($b=0$) with an energy $E_K=3$ eV.

Additional insight is obtained by examination of the potential energy U as a function of time during the collision process. While the total energy varies less than 0.03 eV during the whole event, U, and consequently the kinetic energy delivered to the cluster vibration modes, varies significantly in time. In Fig. 6 we illustrate the evolution of U for center of mass impact ($b=0$) and an initial kinetic energy of 3 eV, for a single silver atom (upper panel) and for a single copper atom projectile (lower panel), on the Au_{12} cluster target. It is observed that U initially diminishes, as the atom approaches the vicinity of the cluster, until it reaches equilibrium at ~150 fs. During the next ~50 fs the projectile closes in on the cluster increasing U and reducing its kinetic energy, until it stops the approach completely at ~200 fs. Thereafter projectile and target start to oscillate, while the energy spreads all over the cluster.

4. Bimetallic structures

Another central objective of this work is to obtain putative ground-state conformations of dilute Au_NAg and Au_NCu nanoalloys, ($N<13$). Traditionally, this objective is approached searching for the minimum energy configuration, thus limiting the scope of the search. However, photo-emission spectroscopy experiments, even of the rather small Au_{10} cluster, identify at least four different low lying energy isomers [35]. Also, it is a fair guess that, for larger bimetallic clusters, the coexistence of various isomers at finite temperatures should increase.

The fabrication of both pristine and alloyed nanoclusters is approached with several different techniques, mainly synthesis [36] (reviewed in detail by Wilcoxon and Abrams [37]) and laser ablation [38–40], which is often used in the fabrication of noble metal nanoclusters [41]. Since the ablation process implies high temperatures it will inevitably mix all the cluster conformations that differ in energy by less than the thermal energy. It is thus quite relevant to have reliable information on a diverse set of local minimum energy nanostructures in order to interpret the experimental results. Moreover, quasi-random mixtures of atoms, that form nanoalloys, have significantly different properties from clusters where one of the species segregates to the surface, as the cluster adopts a core-shell structure [42]. In addition, tuning size, shape, composition, and interface structure of nanoalloys are a key factor for their applications as magnetic, catalytic, and optical materials. Therefore, it is of interest to extend the quest for the minimum energy configuration to a diverse bank of local minima, as those illustrated in Figs. 2 and 3. Among these minima, the lowest energy ones are illustrated in Figs. 7 and 8, for the Au_NAg and Au_NCu clusters, respectively. They are labeled, ordered from lowest to higher energies, as 13-I, 13-II, 13-III and 13-IV. There are cases where two ground state configurations lie so close in energy that they are within the margin of error of the calculation, and we denote them by 13-Ia and 13-Ib. The same convention applies to 12 atom clusters obtained by the above described collision processes.

It is worth noticing that the accepted Au_{13} ground-state found in the literature [15] has the configuration we obtained after the collision of a Ag projectile on a Au target for $E_K=1$ eV, $b=2$, 3, 4 and 5 Å (planar pine-tree like shape). Although we find this same conformation for $Au_{12}Ag$ and $Au_{12}Cu$, they do not correspond to the lowest energy ones. Instead, other similar planar structures turned out to have lower energies, with the exception of $Au_{12}Ag^{I}$ and $Au_{12}Cu^{IV}$. On the other hand, a homotopic transformation describes a continuous deformation of one structure into another. Thus, these conformations are homotops since they have almost the same geometry, but just a different location of the Ag or Cu atom once it is incorporated in the 13 atom cluster.

While the interatomic distances are given in Tables 1 and 2 provides the initial energy E_K, impact parameter b and binding energy per atom E_b of the isomers in Figs. 7 and 8 (notice that $E_b<0$ denotes stable configurations). The E_b values are very similar for all the members of a particular series, implying that to compare with experiment a large number of isomers has to be considered [35].

In Figs. 7 and 8 we indicate several interatomic distances, mainly related to the dopant atom of the cluster (Ag or Cu). Thus, at this point it is of interest to compare with the dimer distances of Au, Ag, and Cu, as well as their combinations which we calculated and tabulated in Table 1. As expected, the dimer separation is slightly smaller than the corresponding ones when the same pair forms part of a cluster.

To the best of our knowledge, there exist only a few related studies of bimetallic AuAg and AuCu clusters. These studies cover different concentrations of atomic species [43], and/or were modeled on the basis of a semi-classical approach [33,34]. However, it is instructive to compare with the general features of these results, focusing on size and concentration differences. Bonačić-Koutecký et al. [43], performed a DFT study of Ag–Au bimetallic clusters of up to 20 atoms, focusing on Au_NAg_N (with $N\leq10$), finding a large s–d hybridization for Au, which is absent for Ag. They also found that Ag atoms are prone to transfer some of their charge to Au atoms. Our results agree with both features which -in our case- also apply to Au_NCu clusters. Bonačić-Koutecký et al. [43] also found hetero-bonds energetically favorable as compared with homo-bonds, a feature we obtained for Cu but not for Ag, where the opposite occurs. This difference can be due to the our low Ag concentration, which is not sufficient to yield a minimal energy 3D ground-state geometry.

Huang et al. [44] recently published an experimental/DFT study of gold clusters, including Au_NAg^- and Au_NCu^-, for $N=6$ and 7. They found that these structures are similar to pure neutral planar gold structures, with the Ag or Cu atom preferring the site with largest coordination. Our results for Au_NAg and Au_NCu also favor planar configurations, just as Huang et al. [44]. However, we found that -for larger clusters- the Ag atom prefers a peripheral site, while the Cu atom chooses sites with coordination larger than the cluster average, but lower than the maximal.

Rapallo, Rossi et al. [33,34] used a semi-classical approach focusing their interest on 34 and 38 atom AuCu clusters, finding an important distortion compared to the pristine Au cluster and a clear tendency of Au to segregate to the surface, leaving the Cu at the core. On the contrary, for Au–Ag clusters the Ag atoms segregate to the

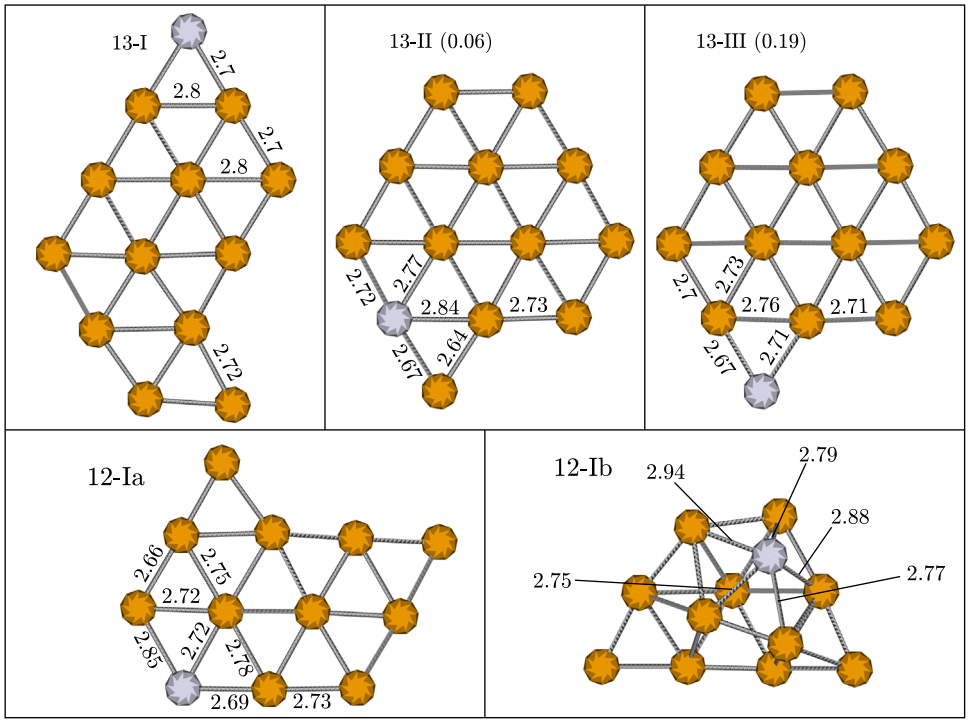

Fig. 7. Ground-state (I) and some low energy isomers (II, III) of $Au_{12}Ag$ (upper panels) and $Au_{11}Ag$. The energy difference in eV is in parenthesis. The small numbers are representative distances in Å.

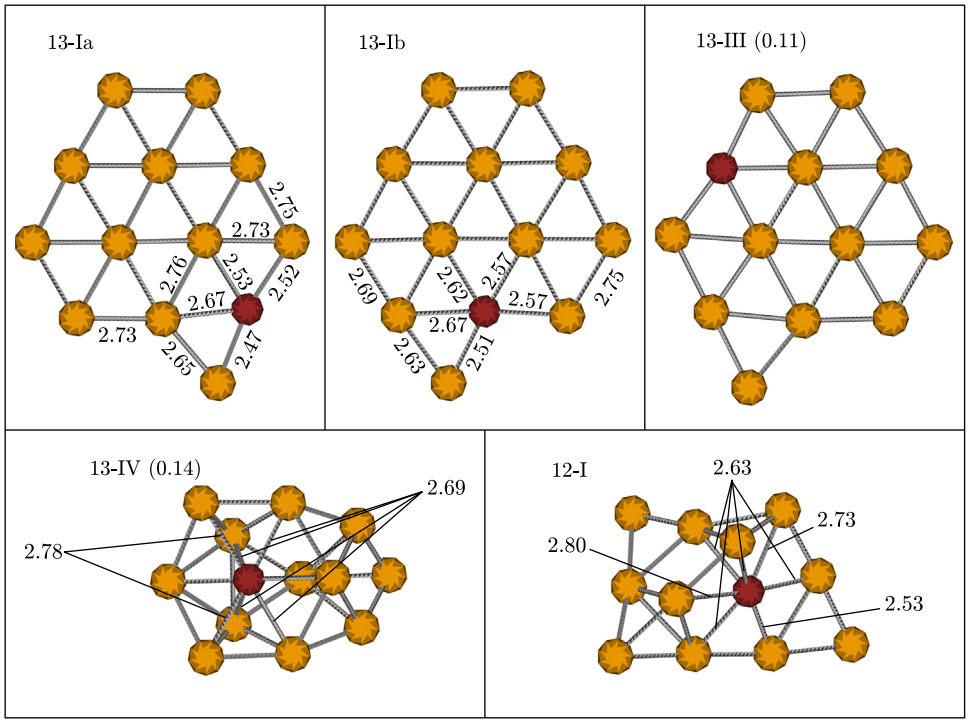

Fig. 8. Ground-state (I) and some low energy isomers (II–IV) of $Au_{12}Cu$ (upper panels) and $Au_{11}Cu$. The energy difference with the ground-state, in eV, is in parenthesis. The small numbers are representative distances in Å.

surface. In the limit of low Ag and Cu concentration their results and ours are in qualitative agreement.

5. Comparison of collision versus DFT results

To search for a set of minimum energy N-atom cluster structures, we generate M highly compressed configurations at random, in a small $(1\times1\times1)$ Å^3 box in the spirit of a Big Bang procedure. Next each configuration is allowed to evolve using the Fast Inertial Relaxation Engine (FIRE) with a phenomenological potential until the largest absolute value of the force acting on every atom is less than the required accuracy, in our case 10^{-9} eV/Å. The FIRE algorithm, as described by Bitzek et al. [11], is a minimization method based on conventional molecular dynamics with velocity modifications and adaptive time steps. Each final structure, which

Table 1
Interatomic distances of Au, Ag and Cu dimers and their binary combinations.

Species	d [Å]
Au–Au	2.52
Ag–Ag	2.58
Cu–Cu	2.22
Au–Ag	2.55
Au–Cu	2.35
Ag–Cu	2.40

Table 2
Structure name, impact parameter b in Å, projectile kinetic E_K in eV and binding energy E_b in eV per atom.

Structure	b	E_K	E_b
$Au_{12}Ag^{I}$	3	4	−2.102
$Au_{12}Ag^{II}$	2	2	−2.097
$Au_{12}Ag^{III}$	1	1	−2.087
$Au_{11}Ag^{Ia}$	2	6	−2.063
$Au_{11}Ag^{Ib}$	1	5	−2.063
$Au_{12}Cu^{I}$	3	3	−2.151
$Au_{12}Cu^{II}$	0	1	−2.151
$Au_{12}Cu^{III}$	3	4	−2.147
$Au_{12}Cu^{IV}$	1	4	−2.143
$Au_{11}Cu^{I}$	2	8	−2.136

we define as a "local minimum structure", is added to the "local minimum structure bank" if the cluster is different from all the ones already included in the bank; otherwise it is discarded. The difference between the cluster configurations is determined by comparing their energies, allowing for a tolerance of $\Delta E < 10^{-7}$ eV. This procedure is repeated for the M initial random configurations to obtain a set of M' minimal structures, where $M' \leq M$. In our case we adopted the value of $M = 10^7$.

We now briefly compare the minimal energy configurations generated by means of collision processes with a massive DFT minimization of the low energy configurations obtained using the Fast Inertial Relaxation Engine (FIRE) procedure (the details of the implementation of the FIRE based energy minimization method used here will be reported elsewhere shortly). For the time being, we just mention that a bank of 4483 different low lying energy $Au_{12}Ag$ and 4483 $Au_{12}Cu$ configurations were generated using FIRE in combination with the Gupta potential [45,46]. Next, all of these 8966 structures were refined quantum mechanically by means of the VASP DFT code. The details of the VASP calculations we carried out to minimize the Gupta generated bank of low lying configurations are the same as described above (see Section 2), but we relaxed somewhat the minimum force requirement to 0.03 eV/Å, in order to carry out these computations within a reasonable amount of time. Our results are illustrated in Fig. 9 which provides a histogram of the number of 3-D clusters lying in a certain energy interval (yellow), and lines specifying the energy values for the 2-D (black) and 3-D (red dashed) collision results. It is apparent that the lowest energies are reached by means of a collision processes. Therefore, this procedure proves superior and seems a promising approach to obtain minimum energy configurations, especially when dealing with planar binary cluster structures.

While the FIRE-based method is a powerful tool to find a large number of different minimum structures, it has an important caveat: the seeds used for the DFT refinement are obtained semi-classically (in our case using the Gupta potential). However, the Gupta derived 2-D structures are either unstable or -at best- they lie much higher in energy. On the other hand, collisions do not face this problem: they yield 2D or 3D structures, since the entire procedure is DFT-based. It is interesting to note that even 3D

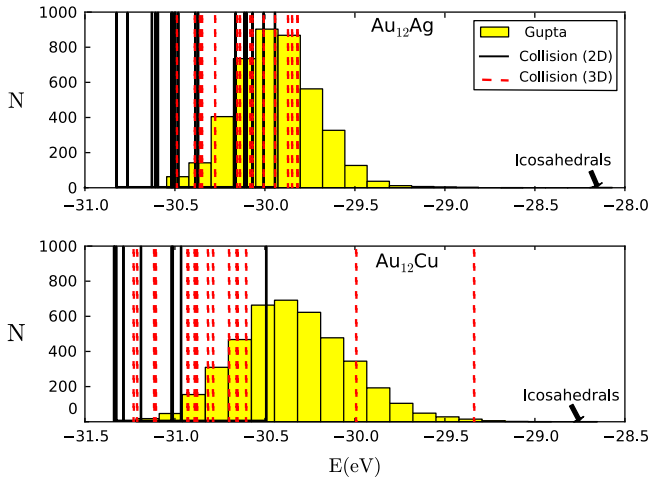

Fig. 9. Histogram of the number N of VASP refined Gupta structures generated by the FIRE method (yellow). In addition the position of the energy values that result from collision processes are denoted by black lines for the 2-D, and dashed-red for the 3-D, $Au_{12}Ag$ and $Au_{12}Cu$ structures. The energy of the DFT calculated classically favored icosahedral configurations, which is quite large, are also indicated. (For interpretation of the references to color in this figure caption, the reader is referred to the web version of this article.)

structures generated by collisions are roughly as good as the ones obtained from the FIRE-based algorithm, confirming our statement above.

It is also interesting to mention that the possibility of tailoring the 0.8 eV energy barrier for the 2D to 3D transition, by substitution of a single gold atom by another noble metal, mentioned in the introduction, is verified by inspection of Fig. 9, where it is apparent that the barrier is reduced to ~0.3 eV for $Au_{12}Ag$ and to ~0.2 eV for $Au_{12}Cu$.

6. Summary and conclusions

In summary, we have implemented a DFT-molecular dynamics study of coinage metal collision processes with two main objectives in mind: (i) contribute to the understanding of the dynamics of the collision process; and (ii) to develop an unbiased procedure to generate a bank of low energy cluster conformations.

In relation to the dynamics of the collision we determined that fusion of projectile and target is the dominant scenario. However, for large energies and impact parameters scattering and cluster fragmentation also do take place. It is interesting to notice that the outcome of the scattering versus fragmentation channels is determined during the initial stages of the simulation, and thus the process is quasi-instantaneous. While Ag projectiles favor fragmentation Cu favors scattering due to its smaller mass, and depending non-trivially on the magnitude of the impact parameter. Schematically, on the basis of statistics, the output can be described by the larger the projectile mass the larger the probability to achieve fusion, while smaller projectile mass favors scattering. Fragmentation is mainly determined by the projectile energy.

On the other hand, we used the collision processes to generate a diverse set of local energy minima, and the putative global minimum of cluster conformations. Our results constitute a clear indication that the use of phenomenological potentials (*i.e.* the exploration of the potential energy surface), to obtain local and global minima is not adequate to generate the quantum mechanical minima of planar conformations. Even after a large amount of seeds are subject to DFT optimization they do not lead to the right conformations, in particular missing completely the planar ones.

In fact, we compared these results with those that are obtained using the Fast Inertial Relaxation Engine (FIRE) in combination with ~5000 VASP refined Gupta potential phenomenological cluster structures, to find that in similar computer time collisions yield lower lying minima, as well as planar configurations. Thus, the use of DFT-MD simulations of collision processes emerges as a powerful tool to find the putative global energy minimum, but also the legion of low lying local energy minima for small clusters.

Our procedure turns out to be specially suited to treat binary systems, given the enormous number of possible configurations a doped cluster can adopt. This way a set of close lying low energy states is generated, which is relevant due to the fact that finite temperature experiments often show the presence of several isomers, rather than a single minimum energy conformation. Moreover, we find that there is an extra bonus: collisions yield planar lower energy structures which cannot be reached by means of phenomenological potential treatments, which favor quasi-spherical geometries, while often small clusters do adopt planar configurations. In our case most of the Ag and Cu doped Au clusters preserve the planar structure of Au_{13} with a Ag or Cu atom substituting for a Au one. As already described by Bonačić-Koutecký et al. [43] during these processes a large $s-d$ hybridization is observed, as well as a significant charge transfer from Au to Ag or Cu.

These results have relevant implications for the interpretation of experimental data, since clusters are created and handled at finite temperatures (*e.g.* by synthesis or laser ablation) and a large set of the local minima configurations often differ from the putative global minimum by less than the corresponding thermal energy [26]. Actually, Koskinen et al. [6] studied the 2D to 3D transition of small Au clusters in the liquid state and found a dynamic coexistence of planar and higher energy volumetric configurations. This is related to narrow basins of attraction of the 2D state, from which the system pops in and out into the larger energy 3D configuration. Thus, the global minimum may be less relevant than the distribution of local minima we have obtained by means of our procedure, when analyzing the experimental data.

Acknowledgments

Supported by the *Fondo Nacional de Investigaciones Científicas y Tecnológicas* (FONDECYT, Chile) under grants 11110510 (FM), 1090225 and 1120399 (MK and JR), 1110135 (JAV) and *Financiamiento Basal para Centros Científicos y Tecnológicos de Excelencia*.

References

[1] A. Sanchez, S. Abbet, U. Heiz, W.D. Schneider, H. Häkkinen, R.N. Barnett, U. Landman, J. Phys. Chem. A 103 (1999) 9573.
[2] M. Valden, X. Lai, D.W. Goodman, Science 281 (1998) 1647.
[3] Y.P. Lee, Y.V. Kudryavtsev, V.V. Nemoshkalenko, R. Gontarz, J.Y. Rhee, Phys. Rev. B 67 (2003) 104424.
[4] K. Takanashi, S. Mitani, M. Sano, H. Fujimori, H. Nakajima, A. Osawa, Appl. Phys. Lett. 67 (1995) 1016.
[5] K. Takanashi, S. Mitani, K. Himi, H. Fujimori, Appl. Phys. Lett. 72 (1998) 737.
[6] P. Koskinen, H. Häkkinen, B. Huber, B. von Issendor, M. Moseler, Phys. Rev. Lett. 98 (2007) 015701.
[7] Marcelo M. Mariscal, Sergio A. Dassie, Ezequiel P.M. Leiva, J. Chem. Phys 123 (November (18)) (2005) 184505.
[8] J. Rogan, R. Ramírez, A.H. Romero, M. Kiwi, Eur. Phys. J. D 28 (2004) 219.
[9] F. Muñoz, J. Rogan, G. García, M. Ramírez, J.A. Valdivia, R. Ramírez, M. Kiwi, Eur. Phys. J. D 61 (2011) 87.
[10] F. Muñoz, J. Rogan, G. García, J.A. Valdivia, R. Ramírez, M. Kiwi, Eur. Phys. J. D 64 (2011) 45.
[11] E. Bitzek, P. Koskinen, F. Gähler, M. Moseler, P. Gumbsch, Phys. Rev. Lett. 97 (2006) 170201.
[12] H. Häkkinen, Chem. Soc. Rev. 37 (9) (2008) 1847.
[13] L. Xiao, L. Wang, Chem. Phys. Lett. 392 (2004) 452.
[14] X. Xing, B. Yoon, U. Landman, J.H. Parks, Phys. Rev. B 74 (16) (2006) 165423.
[15] L. Xiao, B. Tollberg, X. Hu, L. Wang, J. Chem. Phys. 124 (2006) 114309.
[16] E.M. Fernández, J.M. Soler, I.L. Garzón, L.C. Balbás, Phys. Rev. B 70 (2004) 165403.
[17] P. Hohenberg, W. Kohn, Phys. Rev. B 136 (1964) 834.
[18] W. Kohn, L.J. Sham, Phys. Rev. A 140 (1965) 1133.
[19] G. Kresse, J. Hafner, Phys. Rev. B 47 (1993) 558.
[20] G. Kresse, J. Furthmüller, Comput. Mat. Sci. 6 (1996) 15.
[21] G. Kresse, J. Furthmüller, Phys. Rev. B 54 (1996) 11169.
[22] G. Kresse, D. Joubert, Phys. Rev. B 59 (1999) 1758.
[23] J.P. Perdew, K. Burke, M. Ernzerhof, Phys. Rev. Lett. 77 (1996) 3865.
[24] B. Assadollahzadeha, P. Schwerdtfegera, J. Chem. Phys. 131 (2009) 064306.
[25] X. Li, H. Wang, X. Yang, Z. Zhu, J. Chem. Phys. 126 (2007) 084505.
[26] W. Huang, L.S. Wang, Phys. Rev. Lett. 102 (2009) 153401.
[27] J.C. Idrobo, W. Walkosz, S.F. Yip, S. Öğüt, J. Wang, J. Jellinek, Phys. Rev. B 76 (20) (2007) 205422.
[28] Y. Dong, M. Springborg, Eur. Phys. J. D 43 (2006) 15.
[29] J. Wang, G. Wang, J. Zhao, Phys. Rev. B 66 (2002) 035418.
[30] M.P. Johansson, A. Lechtken, D. Schooss, M.M. Kappes, F. Furche, Phys. Rev. A 77 (2008) 053202.
[31] W. Luo, S.J. Pennycook, S.T. Pantelides, Nano Lett. 7 (10) (2007) 3134.
[32] H. Häkkinen, M. Moseler, U. Landman, Phys. Rev. Lett. 89 (2002) 033401.
[33] A. Rapallo, G. Rossi, R. Ferrando, A. Fortunelli, B.C. Curley, L.D. Lloyd, G.M. Tarbuck, R.L. Johnston, J. Chem. Phys. 122 (2005) 194308.
[34] G. Rossi, R. Ferrando, A. Rapallo, A. Fortunelli, B.C. Curley, L.D. Lloyd, R.L. Johnston, J. Chem. Phys. 122 (2005) 194309.
[35] W. Huang, L.S. Wang, Phys. Chem. Chem. Phys 11 (2009) 2663.
[36] E. Messina, L. D'Urso, E. Fazio, C. Satriano, M.G. Donato, C. D'Andrea, O.M. Maragò, P.G. Gucciardi, G. Compagnini, F. Neri, J. Quant. Spectrosc. Radiat. Transfer 113 (2012) 2490.
[37] J.P. Wilcoxon, B.L. Abrams, Chem. Soc. Rev. 35 (2006) 1162.
[38] L.V. Zhigilei, Appl. Phys. A 76 (2003) 339.
[39] E.M. Peña-Méndez, J.R. Hernandez-Fernaud, R. Nagender, J. Houska, J. Havel, Chem. Listy 102 (2008) s1394.
[40] S. Vučković, M. Svanqvist, V.N. Popok, Rev. Sci. Instrum. 79 (2008) 073303.
[41] J. Li, J. Liu, Y. Chen, J. Mass Spectrom. 47 (2012) 620.
[42] R. González, G. García, J.A. Valdivia, R. Ramírez, M. Kiwi, T. Rahman, Phys. Rev. B 83 (2011) 155425.
[43] V. Bonačić-Koutecky`, J. Burda, R. Mitrić, M. Ge, G. Zampella, P. Fantucci, J. Chem. Phys. 117 (2002) 3120.
[44] W. Huang, R. Pal, L.M. Wang, X.C. Zeng, L.S. Wang, J. Chem. Phys. 132 (2010) 054305.
[45] R.P. Gupta, Phys. Rev. 23 (1985) 6265.
[46] F. Cleri, V. Rosato, Phys. Rev. B 48 (1993) 22.